China Ocean Eng., 2020, Vol. 34, No. 6, P. 881–888
DOI: https://doi.org/10.1007/s13344-020-0080-y, ISSN 0890-5487
http://www.chinaoceanengin.cn/ E-mail: coe@nhri.cn

Salinity Distribution at Canal Istanbul and Its Possible Impacts on the Northern Marmara Sea

Şehriban SAÇU*, Tarkan ERDIK, Olgay ŞEN

Istanbul Technical University, Maslak, Istanbul 34467, Turkey

Received February 9, 2020; revised August 1, 2020; accepted September 15, 2020

Abstract

Turkey has announced its plan to construct a new waterway, Canal Istanbul, parallel to the Bosphorus. In this study, the influence of Canal Istanbul on salinity distribution in the northern Marmara Sea is investigated using a previously calibrated 3D hydrodynamic and salinity model. Moreover, the salinity field of the canal and its propagation are examined based on various meteorological cases. Finally, the flow structure of the canal is determined. It is calculated that at the southern end of the canal, mainly unidirectional flow (from the Black Sea to the Marmara Sea) occurs during 68% of the simulation period. A two-layer flow is seen only 28% of the time with a weak lower layer flow, whereas this value decreases to 4% at the north end of the canal. In the southward direction (to the Marmara Sea), velocities higher than 1.5 m/s are rarely observed along the canal. The average surface salinity difference in the northern Marmara Sea due to the construction of the canal is calculated to be smaller than 0.50 ppt. The salinity difference gradually diminishes as water depth increases and after 25 m (from the surface) almost no difference is observed.

Key words: Canal Istanbul, Marmara Sea, salinity distribution, hydrodynamic modeling

Citation: Saçu, Ş., Erdik, T., Şen, O., 2020. Salinity distribution at Canal Istanbul and its possible impacts on the northern Marmara Sea. China Ocean Eng., 34(6): 881–888, doi: https://doi.org/10.1007/s13344-020-0080-y

1 Introduction

The Bosphorus is a unique waterway that connects the European and Asian continents. The strait is a natural channel that provides water transfer between the Black Sea and the Marmara Sea and, therefore, the Mediterranean Sea. Being the only passage connecting the Black Sea to the open seas, it is of vital importance not only for Turkey but also for the neighboring countries of the Black Sea. The Bosphorus plays a significant role in the social, environmental, strategic and economic issues of the metropolitan city of Istanbul in the past and present. It is one of the narrowest and busiest maritime routes for international navigation (Ertürk and Yönsel, 2002). Beside its extraordinary maritime traffic, the Bosphorus presents a unique flow structure that has attracted the attention of oceanographers for many decades.

The Bosphorus has a complex geometry characterized by sharp turns, irregular coastlines, sills and narrows. It is approximately 31 km in length and has a varying width of between 0.7 km and 3.5 km, with an average of 1.6 km. The bathymetry of the Bosphorus also shows abrupt changes, while the average depth is 40 m along the whole strait. The depth increases up to 100 m at the narrowest section and decreases to 30 m near the Golden Horn. There are two sills in the strait, one in the north and the other in the south. The northern sill is located at the Black Sea end of the Bosphorus with a depth of about 60 m. The southern sill is located at the Marmara Sea end of the Bosphorus and is nearly 30 m deep.

The Bosphorus presents a stratified two-layer flow structure. The brackish water of the Black Sea flows to the south in the upper layer, and the salty water from the Marmara Sea flows to the north in the lower layer. The upper layer flow originates from the water level difference between the Black and Marmara seas. River discharges to the Black Sea with precipitation exceed evaporation rates, cause a net outflow from the Black Sea through the Bosphorus (Peneva et al., 2001; Kara et al., 2008). The evaporation rates of the Mediterranean and Marmara seas are higher compared with the Black Sea, which results in salinity differences. The density variations originating from salinity differences cause the lower layer flow from the Marmara Sea to the Black Sea (Oğuz and Sur, 1989; Özsoy et al., 1988; Oğuz, 2005; Jarosz et al., 2011; Ilıcak et al., 2009; Stanev et al., 2017; Erdik et al., 2018, 2019; Öztürk et al., 2012). The water level difference between the two ends of the Bosphorus fluctuates between −0.25 and 0.65 m according to hourly water level data, where negative value means

*Corresponding author. E-mail: sacus@itu.edu.tr

the water level of the Marmara Sea is higher than that of the Black Sea and vice versa (Saçu et al, 2020). The tide is small in amplitude only about 2 cm and not an important fluctuation in the Bosphorus (Yüce, 1993; Yüce and Alpar, 1994; Andersen et al., 1997). The mean upper layer salinity at the north end of the Bosphorus is 18 ppt, and it increases gradually to 23−25 ppt at the south exit. The lower layer salinity is about 38 ppt at the Marmara Sea end of the Bosphorus, and it decreases to 33 ppt at the Black Sea entrance of the Bosphorus (Sur et al., 2004, 2005).

Turkey announced the Canal Istanbul Project, claiming that an alternative and safe route in addition to the natural one is needed to overcome heavy traffic in the Bosphorus and protect the historical city from accidents. The advantages and disadvantages of the project have been actively discussed, with major concerns especially regarding the Montreux Convention, which regulates the passage of merchant and warships through Turkish Straits and environmental issues. Sözer and Özsoy (2017) stated that the hydrodynamic and environmental effects of a human-made second channel constitute a major anxiety for marine biologists and oceanographers due to the announcement of the project. Even though the potential concerns in the Marmara Sea can be addressed using hydrodynamic models, only a few studies have been performed so far in this regard; such studies can shed light on rational discussion and objective evaluation. In this study, a 3D hydrodynamic and salinity model was applied using a previously calibrated model to determine the flow structure and salinity of the canal, which is assumed to have a constant width of 300 m and depth of 25 m. Besides, the impact of the Canal on salinity distribution across the northern Marmara Sea is investigated.

2 Model description

In this study, Deflt3D-Flow is applied, which was developed by Deltares. It implies 2D or 3D simulations of non-steady flow and transport phenomena that mainly resulted from tidal and meteorological forcing; besides, it includes the effect of the density differences due to non-uniform salinity and temperature distribution. It solves non-steady shallow water equations derived from Navier Stokes equations for incompressible free-surface flows. Delft3D has been previously applied in many open sea and coastal area cases: Arabian Gulf (Elhakeem et al., 2015), Pentland Firth (Rahman and Venugopal, 2017), Cádiz Bay (Zarzuelo et al., 2017), Columbia River Estuary (Sandbach et al., 2018), Yangtze Estuary (Zhang et al., 2018), and Bosphorus (Erdik et al., 2018, 2019; Şen et al., 2019). For further details, readers are referred to Delft3D-Flow User Manual Deltares (Deltares, 2013).

3 Model development

The model domain is covering an area between ~ 41.42°N, 29.72°E at the Black Sea side and ~ 40.80°N, 28.20°E at the Marmara Sea side. The model consists of 2423 orthogonal grid cells in the horizontal dimesion (6 cells at the narrowest section). In the vertical, *Z*-model approach with 20 layers is selected since σ-model may stay insufficient in modeling of the stratified flows over steep bottom topography and *Z*-model decreases artificial mixing (Deltares, 2013). There are two open boundaries, which are the Black Sea open boundary in the north and the Marmara Sea open boundary in the south. In the open boundaries, the model is forced by uniformly distributed hourly water level measurements conducted by TAISEI (RTMEU, 2005). As for salinity and temperature data, monthly measurements performed by Istanbul Water Sewerage Administration (ISKI) at Stations M23 and M24 (Fig. 1) are used at the southern boundary, while monthly data by Copernicus "Global Ocean Physics Reanalysis" at Point C is used at the northern boundary. Meteorological data were obtained from the European Center for Medium-Range Weather Forecasts (ECMWF) as 6-hourly wind velocity and air pressure data with spatial resolution of 0.125° and it was apllied across the model domain. The bathymetric coastline data are provided from the Turkish Naval Forces Office of Naviga-

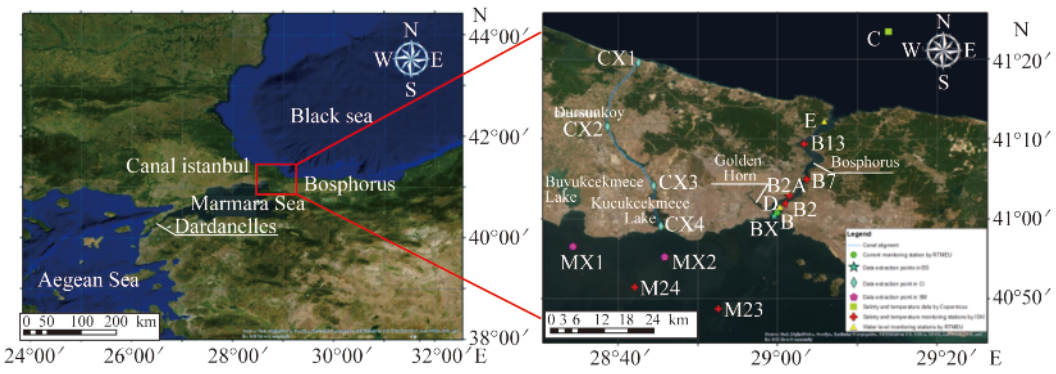

Fig. 1. Monthly salinity and temperature measurement stations B2A, B7, B13, M23 and M24 performed by ISKI (red crosses); monthly salinity and temperature data point C by Copernicus product (green box); water level monitoring stations D and E by RTMEU (yellow triangles); current velocity station B by RTMEU (green circle); data extraction point in the Bosphorus BX (cyan star); data extraction point in the canal CX1, CX2, CX3, and CX4 (cyan diamonds); data extraction points in the Marmara Sea MX1 and MX2 (magenta pentagons). The canal route is shown with parallel blue lines.

tion, Hydrography, and Oceanography. Bathymetry of the Black Sea and the Marmara Sea have a scale of 1/300 000 while scale of the Bosphorus is 1/20000.

Initial conditions for the water level and velocity field are set to zero. For salinity and temperature, uniform 38 ppt and 15°C are specified as initial conditions. To obtain a reliable adjustment of the model field and realistic oceanographic conditions, spin-up is performed for 2 weeks.

An intensive calibration process is performed for two months, December 2004 and June 2005, using a previous study (Saçu et al., 2020), and the periods are under the effects of different forcing mechanisms. In December, the flow structure of the Bosphorus is influenced by severe meteorological conditions, whereas in June, the conditions are calm. The calibration of periods under different forcing mechanisms enables the determination of optimum parameters in order to reflect the complex hydrodynamic behavior of the Bosphorus. The model domain is calibrated against hourly current velocity measurements at Station B (Fig. 1) by adjusting wind drag coefficient, bottom friction coefficient, viscosity, and diffusivity (Table 1). In Figs. 2a−2b and 3a−3b, the hourly current velocity at the surface and bottom layers are given as a time series where black and red lines represent predicted and observed values, respectively. The results of the hydrodynamic model show a high agreement between observed and simulated data for both months. To validate the model, current velocity is also investigated for March 2005 where large variations in currents were seen (Figs. 2c and 3c). The model is able to generate current velocity quite well and gives a similar error statistics with studies in the literature such as Öztürk et al. (2012) and Erdik et al. (2019). However, there are some discrepancies between observed and predicted velocities which can be resulted from poor temporal resolution of the salinity and temperature data in open boundaries and low resolution of the batyhmetric data. Beside, the measurement sensor produces noise by itself. For a detailed description of the model and calibration study, readers should refer to the study of Saçu et al. (2020).

The salinity field of the Bosphorus is also calibrated and validated against salinity measurements carried out by ISKI at Stations B2, B2A, B7, and B13 (Fig. 4). A very good

Table 1 Parameters used in the numeric model

Parameter	Specification
Bottom roughness	Constant Manning coefficient of 0.024
Horizontal eddy viscosity	20 m^2/s
Horizontal eddy diffusivity	20 m^2/s
Time step	0.2 s
Turbulence model	$k-\varepsilon$
Vertical eddy diffusivity	1.0×10^{-5} m^2/s
Vertical eddy viscosity	0.000 1 m^2/s
Wind drag coefficients break points (coefficients)	0.001; 0.001 5
Wind drag coefficients break points (wind speed)	0; 3; 100

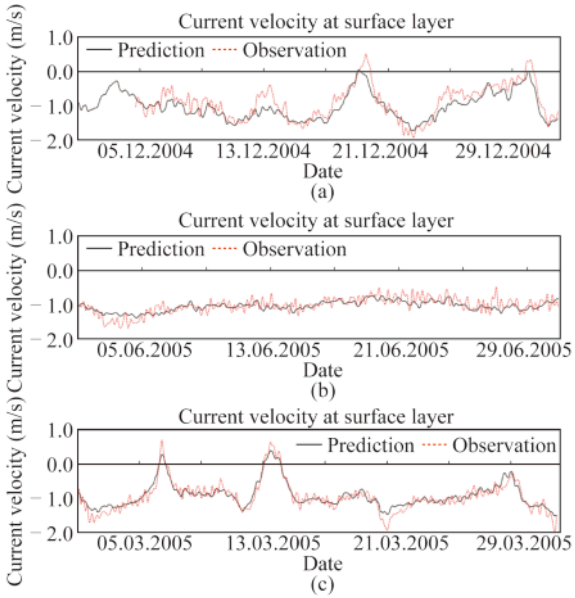

Fig. 2. Surface current velocity in December 2004, June 2005, and March 2005 where the black and red lines indicate predicted and observed values, respectively.

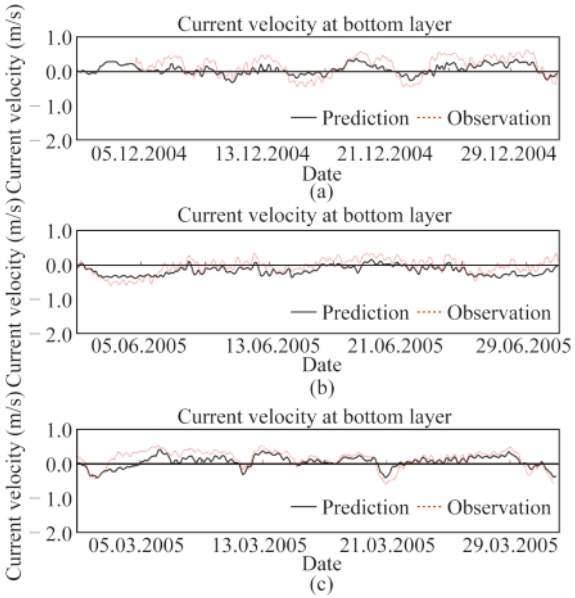

Fig. 3. Bottom current velocity in December 2004, June 2005, and March 2005 where the black and red lines indicate predicted and observed values, respectively.

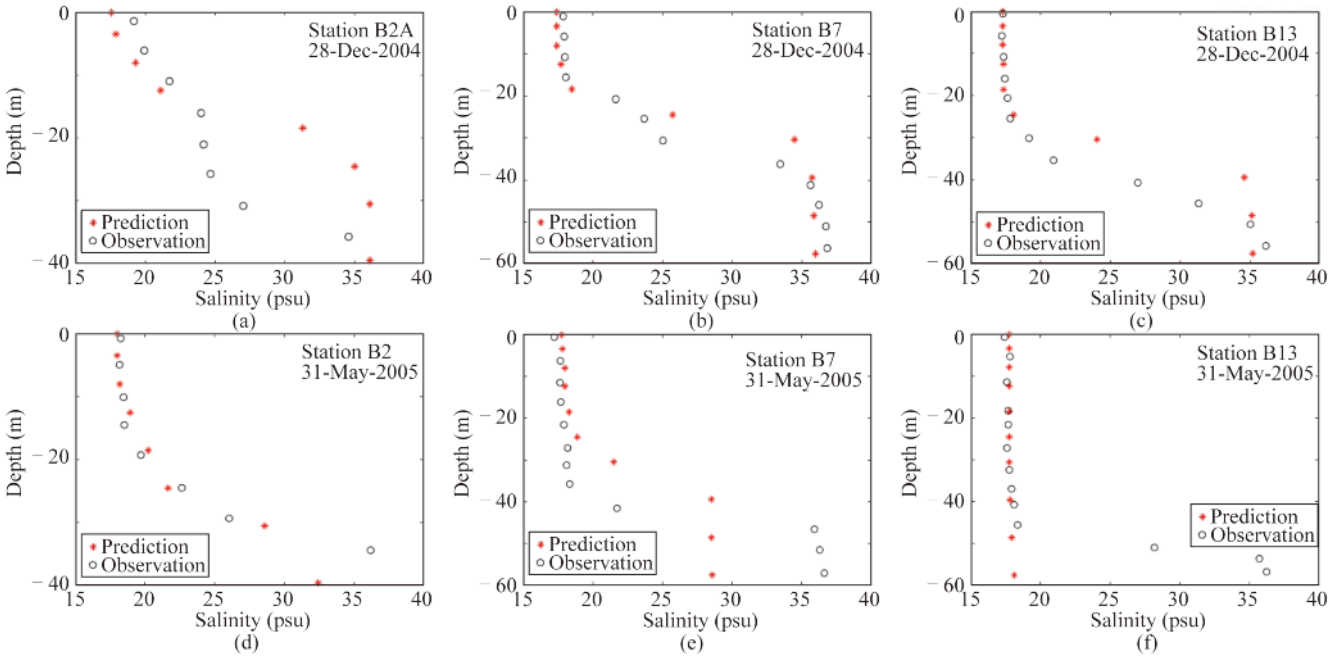

Fig. 4. Predicted and observed salinity profiles, upper and lower panels represent December 2004 and May 2005, respectively.

agreement between model and observations is obtained for the first 35 m from the surface whereas, at larger depths, there are some discrepancies. A similar result is valid also for validation, the model succeeds to estimate salinity near the surface and mid-layer, however it underestimates near the bottom (Fig. 5).

4 Results

The results of the hydrodynamic and salinity model are evaluated between December 2004 and January 2006 after the calibration process.

4.1 Current velocity field at Canal Istanbul

The flow structure of the canal differs from that of the Bosphorus, where, generally, a two-layer stratified flow is seen (Saçu et al., 2020). At the southern part of the canal, mainly unidirectional flow (from the Black Sea to the Marmara Sea) occurs during 68% of the simulation period. A two-layer flow is seen only 28% of the time with a weak lower layer flow, which is also compatible with the idealized model results of Sözer and Özsoy (2017). This value decreases to 4% at the northern entrance of the canal because baroclinic forcing cannot oppose barotropic forcing and there is bottom friction. Similarly, a one-layer flow towards the Black Sea is rarely observed along the canal, 4% of the time, when strong northward winds are seen (generally over 8 m/s). However, it occurs 2.2% of the time in the Bosphorus (Yüksel et al., 2008). This difference shows that the canal is more sensitive to meteorological conditions.

The velocity behavior along the canal is analyzed at the data extraction locations CX1, CX2, CX3, and CX4 in Fig. 1, shown with cyan diamonds, which are located close to the northern end, Dursunköy, Küçükçekmece Lake and southern end of the canal, respectively. The temporal variability of the surface and bottom layer currents in these locations during the simulation period are given in Figs. 6a and 6b, respectively. Negative values indicate a flow direction towards the south (to the Marmara Sea), while positive values represent the northward direction (to the Black Sea).

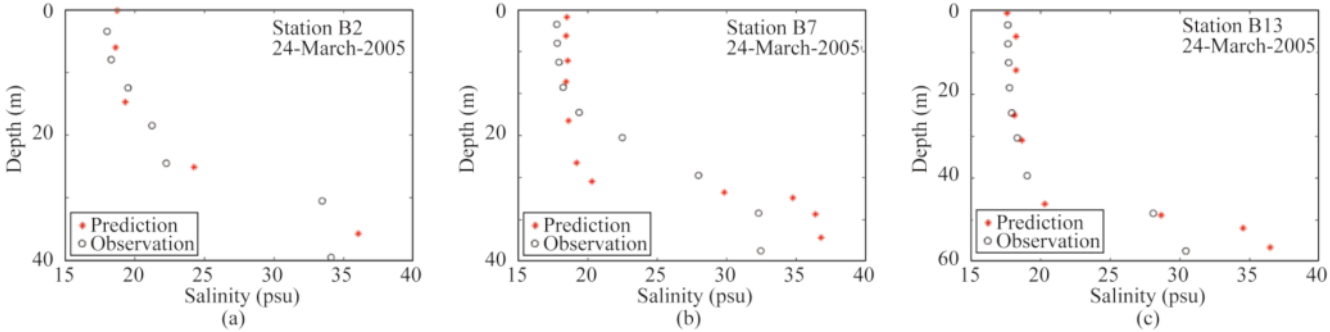

Fig. 5. Predicted and observed salinity profiles at March 2005 for Stations B2, B7, and B13.

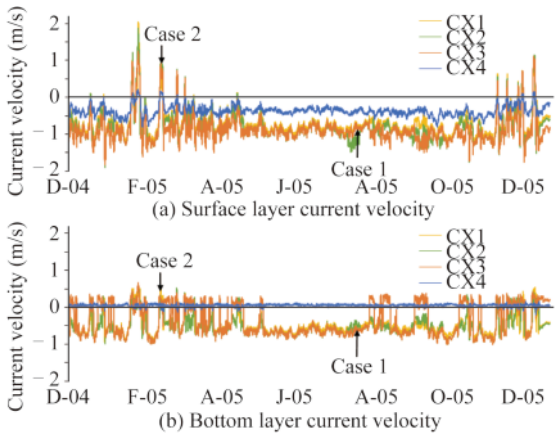

Fig. 6. (a) Surface and (b) bottom layer current velocities in the canal at Points CX1, CX2, CX3, and CX4 during simulation period. Negative values indicate flow direction towards the south (to the Marmara Sea) while positive values represent northward direction (to the Black Sea).

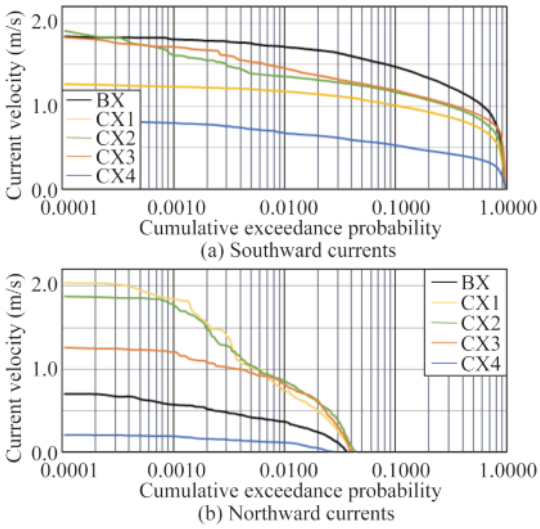

Fig. 7. Cumulative exceedance probability of surface layer current velocity at the southern Bosphorus (BX) and along the canal (CX1, CX2, CX3, and CX4) during simulation period: a) southward currents, b) northward currents.

The surface current velocity along the canal varies between −1.9 and 2.0 m/s, whereas it fluctuates between −1.0 and 0.7 m/s at the bottom. The mean surface current velocities are calculated as −0.7, −0.8, −0.9 and −0.4 m/s at CX1, CX2, CX3 and CX4, respectively, while they are −0.5, −0.5, −0.4, and 0.1 m/s respectively for the same locations at the bottom. The velocity at CX4 is the smallest during the simulation period because of the increasing cross-sectional area at Küçükçekmece Lake. The surface currents follow a calm pattern in the summer, whereas large fluctuations are seen in the winter due to the severe meteorological conditions, which are similar to those in the Bosphorus (Yüksel et al., 2008; Saçu et al., 2020).

The current velocities have a crucial importance regarding shipping facilities since high flow rates can jeopardize maritime traffic and the environment. In Figs. 7a and 7b, the cumulative exceedance probability of the surface layer current velocities along the canal (CX1, CX2, CX3, and CX4) are compared with Point BX, which is extracted at the southern exit of the Bosphorus, where currents reach maximum values (Möller, 1928; Defant, 1961; Gregg and Özsoy, 2002; Oğuz, 2005; Öztürk et al., 2012). In the southward direction (to the Marmara Sea), the exceedance probabilities of 1.5 m/s are 0.3% and 0.68% for CX2 and CX3 respectively, whereas it is 8.46% for BX. At the northern and southern ends of the canal (CX1 and CX4), current velocities are smaller than this value in all time percentages (Fig. 7a). In the northward direction, the exceedance probabilities of 1.5 m/s are 0.21% and 0.19% for CX1 and CX2 respectively, while at CX3, CX4 and BX, velocities under this value appear at all times (Fig. 7b).

4.2 Penetration of saline waters along the Canal Istanbul

Salinity values along the canal are low compared to those of the Bosphorus because majority of the time, a one-layer flow to the south dominates the flow structure. The mean salinity of the north end of the canal is calculated as a uniform value of 18 ppt from surface to bottom, while at the south end, the surface salinity increases to 19 ppt, and the bottom salinity increases to 30 ppt as a result of weak lower layer flow heading to the north in this section.

Barotropic and baroclinic forcing, which are inversely proportional to each other, are responsible for the penetration of salinity in the canal. Density gradients between the Marmara Sea and the Black Sea tend to increase the salinity penetration of the bottom flow, while the strengthened barotropic forcing leads to a decrease in the length; these are similar to the findings of Sözer and Özsoy (2017). In this study, the penetration length (L) and thickness (h) of the lower layer flow are investigated under two different flow conditions in the canal. The first case (Case 1) is selected from a period where currents and meteorological variables follow a calm pattern in the canal. During Case 1 (26 July, 2005), winds are slow and below 2 m/s in the southward direction, where the salinity structure of the canal is under the influence of mainly barotropic forcing originated from the water level differences between the adjacent Black Sea and Marmara Sea. The second case (Case 2) is chosen during a pronounced baroclinic forcing throughout the canal because of the weakened barotropic (and inversely increased baroclinic) forcing by strong winds of over 10 m/s blowing in northward direction (between 13 and 16 February, 2005). Fig. 8 gives the canal wind speed at Point CX1 in Fig. 1, which is obtained from ECMWF (Era-Interim), where positive and negative values represent northward and southward winds, respectively. Wind speed is generally small between April and October. However, it reaches higher values in south/north directions during the other months.

During Case 1, a one-layer flow in the canal appears

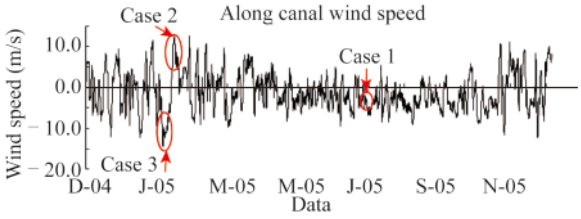

Fig. 8. Time series of wind speed distribution, obtained from ECMWF database at the northern end of the canal, where negative and positive values represent southward and northward directions, respectively.

where brackish waters of the Black Sea flow towards the Marmara Sea along the canal (Fig. 9a). In this case, the salinity between CX3 and CX1 has a uniform value of 18 ppt. Saline waters penetrate into the canal between CX4 and CX3; *h* is 5 m from the bottom. The salinity at the bottom is about 28 ppt, and *L* is about 7 km from the south entrance of the canal.

During Case 2, the change of salinity along the canal is investigated between 13 and 16 February 2005, with one-day time intervals; baroclinic force intensifies with time. On 13 February, a one-layer flow to the Marmara Sea dominates the flow structure along the canal and demonstrates a similar salinity profile with Case 1 (Fig. 9b), with *L* of ~7 km and *h* of 5 m from the bottom; salinity near the bottom is 29 ppt. As the wind speed increases towards the north, barotropic forcing weakens (inversely baroclinic forcing strengthens), and a two layer flow appears. Between 13 and 14 February 2005, the upper layer reversed its direction, and a one-layer flow to the Black Sea appeared. On 14 Feb. (Fig. 9c), a one layer flow structure to the Black Sea dominates the vertical velocity profile. L increases to 25 km, and a 29 ppt salinity front is reached near CX2; the bottom salinity between CX3 and CX4 increases to 31 ppt. On 15 Feb. (Fig. 9d), baroclinic flow intensifies, and a 29 ppt salinity front propagates in the first 35 km of the canal; *h* increases to 10 m from the bottom. The salinity of surface layers also increases to 21 ppt, from the typical value of 18 ppt. On 16 Feb. (Fig. 9e), *L* and *h* increase to 40 km and 15 m respectively. The saline waters reach the north end of the canal, increasing the bottom salinity to 26 ppt. The transition from 13 to 16 Feb., 2005, looks like a propagation of denser waters in the lock exchange experiments by Stanev et al. 2017. This type of transition repeats periodically in winter when barotropic forcing is weakened by strong northward winds, with a backward displacement of the salinity front (to the Marmara Sea) as the barotropic forcing starts to dominate flow structure again.

4.3 Salinity field at northern Marmara Sea

The influence of possible salinity changes on the northern Marmara Sea is analyzed at two points, MX1 and MX2 (Fig. 1), during a considerably long simulation period, where the first point represents the west of the canal and the second one is near the southern exit of the canal. In Fig. 10, the surface salinity differences at MX1 and MX2 (before and after the addition of the canal to the model domain) are shown. The salinity pattern in the summer and autumn periods generally follows a calm pattern, whereas it shows fluctuations in the winter and early spring times, in accordance

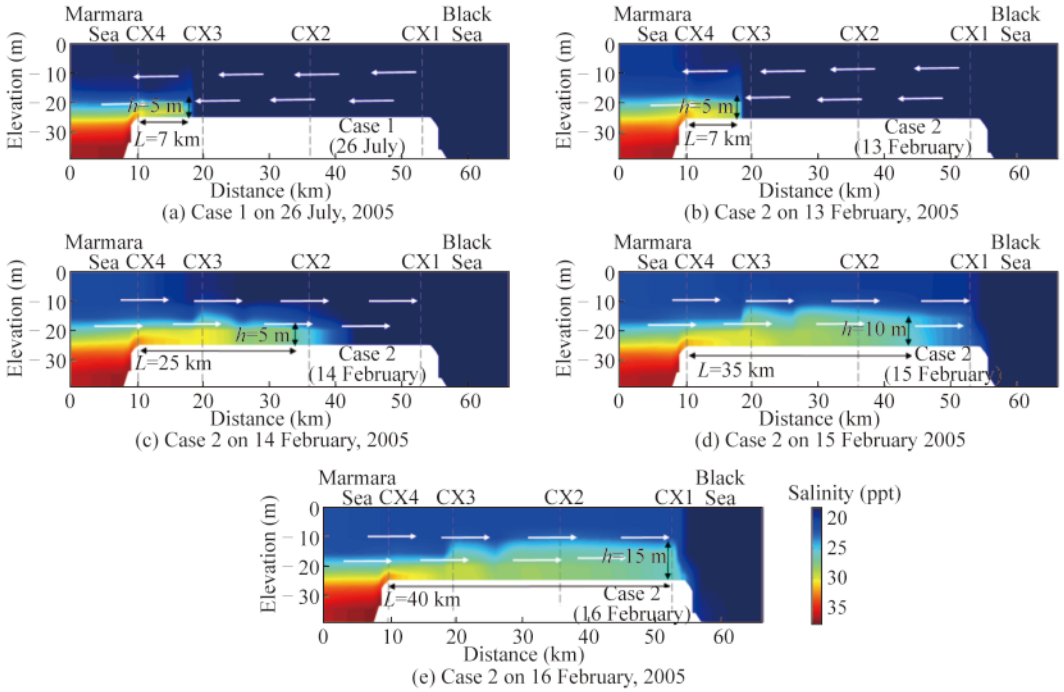

Fig. 9. Salinity profiles along the canal (a) Case 1 on 26 July, 2005; (b) Case 2 on 13 February, 2005; (c) Case 2 on 14 February, 2005; (d) Case 2 on 15 February 2005; (d) Case 2 on 16 February, 2005.

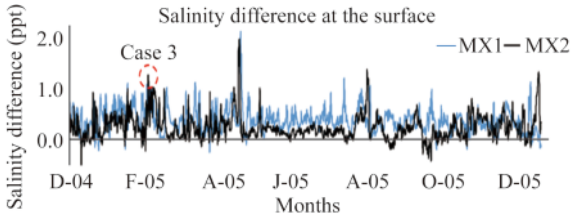

Fig. 10. Surface salinity difference (before and after the addition of the canal to the model domain) at MX1 and MX2 during the simulation period.

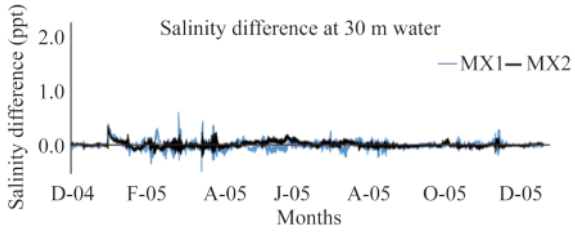

Fig. 11. Salinity difference at the water depth of 30 m (before and after the addition of the canal to the model domain) at MX1 and MX2 during the simulation period.

with the wind speed and current velocity behavior along the canal (Fig. 8 and Fig. 6 respectively). The average surface salinity difference is calculated to be about 0.40 ppt at MX1, while it is smaller at MX2 with a value of 0.25 ppt, with instant maxima salinity differences reaching 2.21 and 2.00 respectively, which shows that the west of the canal will be more affected. Since the location of MX2 is already affected by waters coming from the upper layer flow of the Bosphorus, the salinity difference remains smaller in this region compared to MX1. The salinity difference at 30 m water depth is shown in Fig. 11, which indicates that brackish waters flowing through the canal could not penetrate depths higher than the depth of the canal (25 m).

The spatial distribution of brackish waters originating from the Bosphorus and the canal is investigated for Case 3 (9 Feb., 2005), when the strong southward winds, up to 14 m/s, intensify the barotropic forcing and leads to a one-layer flow to the Marmara Sea both in the canal and Bosphorus, where the brackish water entrainment is very high (Saçu et al., 2020).

The surface salinity distribution with current velocity vectors in the northern Marmara Sea (before and after the addition of the Canal to the model domain) is represented in Figs. 12a and 12b, respectively, during Case 3. The surface flow in Bosphorus with velocity of 1.6 m/s as a turbulent buoyant jet turns anticylconically between Zeytinburnu and Beylikdüzü coasts (Saçu et al., 2020). That spreading behavior generates a relatively more saline area "A", with approximately 1 ppt difference, depicted with dotted line in Fig. 12a. The salinity at the exit of Bosphorus is 18.5 ppt while that increases to 20.5 ppt and 21 ppt at MX1 and MX2, respectively, as a result of horizontal mixing between brackish and saline waters (Fig. 12a). At Fig. 12b, the surface flows exit the Canal with 0.5 m/s and direct to the south. The southward flow of Canal breaks down the previously generated anticyclonic eddy by Bosphorus and forms a new smaller eddy between MX1 and MX2 (Saçu et al., 2020), causing entrance of brackish water to area "A", reducing the salinity difference to 0.5 ppt between the inside and outside of A. The salinity between Beylikdüzü and Zeytinburnu coasts also decreases as a result of secondary brackish water entrainment by Canal. The decrease amount is about 1 ppt and 0.5 ppt at MX1 and MX2, respectively.

5 Conclusion

The intense debate continues on how the proposed canal construction in Istanbul will influence the marine environment in the Marmara Sea. In this study, based on the Delft3D-Flow, a three-dimensional hydrodynamic model for determining the impact of Canal Istanbul on salinity distribution in the northern part of the Marmara Sea is set up. The basic idea behind this study is to address the canal dynamics under different meteorological conditions. The following conclusions can be drawn from the study: (1) The estimates of the numerical model clearly indicate volume flux in the canal from the Black Sea to the Marmara Sea during 68% of the simulation period. (2) The brackish waters of the Black Sea (~18 ppt) dominates the canal. However, under the strong northward wind conditions, the baroclinic flow in the canal intensifies, and a 29 ppt salinity front reaches the Black Sea entrance of the canal. (3) The

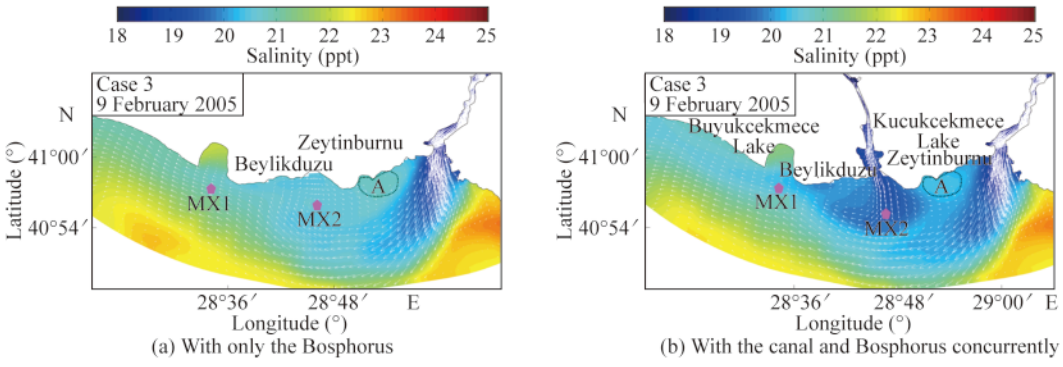

Fig. 12. Surface salinity distribution with current velocity vectors at Case 3 (a) only with the Bosphorus (b) with the canal and Bosphorus concurrently.

mean surface current velocity at the exit of the canal is smaller than 0.5 m/s due to the increasing cross-sectional area at Küçükçekmece Lake. Similar to the conditions in the Bosphorus, surface currents follow a calm pattern in summer, whereas large fluctuations are seen in winter. (4) The average surface salinity difference in the northern Marmara Sea due to the construction of the canal is calculated to be smaller than 0.5 ppt. The salinity difference around 30 m water depth demonstrates that brackish waters of the Black Sea through the canal do not penetrate into the deeper zones.

References

Andersen, S., Jakobsen, F. and Alpar, B., 1997. The water level in the Bosphorus Strait and its dependence on atmospheric forcing, *Deutsche Hydrografische Zeitschrift*, 49(4), 467–476.

Defant, A., 1961. *Physical Oceanography*, Vol. 1, Pergamon, New York.

Deltares, D., 2013. *Delft3D-FLOW User Manual*.

Elhakeem, A., Elshorbagy, W. and Bleninger, T., 2015. Long-term hydrodynamic modeling of the Arabian Gulf, *Marine Pollution Bulletin*, 94(1-2), 19–36.

Erdik, T., Şen, O., Erdik, J.D. and Öztürk, İ., 2018. Long-term 3D hydrodynamic modeling and water surface statistics in marmara sea, *Marine Geodesy*, 41(2), 126–143.

Erdik, T., Şen, O. and Öztürk, İ., 2019. 3D numerical modeling of exchange flows in golden horn estuary, *Journal of Waterway*, *Port*, *Coastal*, *and Ocean Engineering*, 145(5), 04019018.

Ertürk, Ş.N. and Yonsel, F., 2002. An application of the ADAM model for pollution and oil spill tracking in Bosphorus, in: *ISWA Word Environment Congress and Exhibition 2002*, pp.8−12.

Gregg, M. C. and Özsoy, E., 2002. Flow, water mass changes, and hydraulics in the Bosphorus, *Journal of Geophysical Research*: *Oceans*, 107(C3), 2-1–2-23.

Ilıcak, M., Özgökmen, T.M., Özsoy, E. and Fischer, P.F., 2009. Non-hydrostatic modeling of exchange flows across complex geometries, *Ocean Modelling*, 29(3), 159–175.

Jarosz, E., Teague, W.J., Book, J.W. and Beşiktepe, Ş., 2011. On flow variability in the Bosphorus Strait, *Journal of Geophysical Research*: *Oceans*, 116(C8), C08038.

Kara, A.B., Wallcraft, A.J., Hurlburt, H.E. and Stanev, E.V., 2008. Air–sea fluxes and river discharges in the Black Sea with a focus on the Danube and Bosphorus, *Journal of Marine Systems*, 74(1−2), 74–95.

Möller, L., 1928. *Alfred Merz Hydrographiche unter Suchungen in Bosphorus and Dardanalten*, Veroff. Insr. Meeresk, Berlin University, Neue Folge A, 18.

Oğuz, T., 2005. Hydraulic adjustments of the Bosphorus exchange flow, *Geophysical Research Letters*, 32(6), L06604.

Oğuz, T. and Sur, H.I., 1989. A two-layer model of water exchange through the Dardanelles Strait, *Oceanolagica Acta*, 12(1), 23–31.

Özsoy, E., Oğuz, T., Latif, M.A., Ünlüata, Ü., Sur, H.I. and Beşiktepe, S., 1988. *Oceanography of the Turkish Straits—Second Annual Report*, Vol. 1, Institute of Marine Science, Middle East Technical Univ., Erdemli, Turkey.

Öztürk, M., Ayat, B., Aydoğan, B. and Yüksel, Y., 2012. 3D numerical modeling of stratified flows: Case study of the Bosphorus Strait, *Journal of Waterway*, *Port*, *Coastal*, *and Ocean Engineering*, 138(5), 406–419.

Peneva, E., Stanev, E., Belokopytov, V. and Le Traon, P.Y., 2001. Water transport in the Bosphorus Straits estimated from hydro-meteorological and altimeter data: Seasonal to decadal variability, *Journal of Marine Systems*, 31(1−3), 21–33.

Rahman, A. and Venugopal, V., 2017. Parametric analysis of three dimensional flow models applied to tidal energy sites in Scotland, *Estuarine*, *Coastal and Shelf Science*, 189, 17–32.

RTMEU (Republic of Turkey Ministry of Environment and Urbanization), 2005. *Long-Term Continuous Current Velocity Measurements*, RTMEU, Ankara, Turkey.

Saçu, Ş., Erdik, T., Stanev, E.V., Şen, O., Erdik, J.D. and Öztürk, İ., 2020. Hydrodynamics of canal istanbul and its impact in the northern Sea of Marmara under extreme conditions, *Ocean Dynamics*, 70(6), 745–758.

Sandbach, S.D., Nicholas, A.P., Ashworth, P.J., Best, J.L., Keevil, C.E., Parsons, D.R., Prokocki, E.W. and Simpson, C.J., 2018. Hydrodynamic modelling of tidal-fluvial flows in a large river estuary, *Estuarine*, *Coastal and Shelf Science*, 212, 176–188.

Şen, O., Saçu, Ş., Erdik, T., Erdik, J.D. and Öztürk, İ., 2019. Investigation of Northern Bosphorus flow structure with River Danube, *Proceedings of the 9th International Symposium on Atmospheric Sciences*, Istanbul, Turkey, pp. 516-522.

Sözer, A. and Özsoy, E., 2017. Water exchange through Canal İstanbul and Bosphorus Strait, *Mediterranean Marine Science*, 18(1), 77–86.

Stanev, E.V., Grashorn, S. and Zhang, Y.J., 2017. Cascading ocean basins: Numerical simulations of the circulation and interbasin exchange in the Azov-Black-Marmara-Mediterranean Seas system, *Ocean Dynamics*, 67(8), 1003–1025.

Sur, H.İ., Okuş, E., Güven, K.C., Yüksek, A., Altıok, H., Kıratlı, N., ... & Övez, S., 2004. *Water Quality Monitoring Annual Report*, ISKI (The Istanbul Water and Sewage Authority), Istanbul.

Sur, H.İ., Okuş, E., Güven, K.C., Yüksek, A., Altıok, H., Kıratlı, N., ... & Övez, S., 2005. *Water Quality Monitoring Annual Report*, ISKI (The Istanbul Water and Sewage Authority), Istanbul.

Yüce, H., 1993. Water level variations in the Sea of Marmara, *Oceanologica Acta*, 16(4), 335–340.

Yüce, H. and Alpar, B., 1994. Investigation of low frequency sea level changes at the Strait of Istanbul (Bosphorus), *Turkish Journal of Engineering and Environmental Sciences*, 18(3), 233–238.

Yüksel, Y., Ayat, B., Ozturk, M.N., Aydogan, B., Guler, I., Cevik, E.O. and Yalçıner, A.C., 2008. Responses of the stratified flows to their driving conditions—A field study, *Ocean Engineering*, 35(13), 1304–1321.

Zarzuelo, C., López-Ruiz, A., Díez-Minguito, M. and Ortega-Sánchez, M., 2017. Tidal and subtidal hydrodynamics and energetics in a constricted estuary, *Estuarine*, *Coastal and Shelf Science*, 185, 55–68.

Zhang, F.Y., Sun, J., Lin, B.L. and Huang, G.X., 2018. Seasonal hydrodynamic interactions between tidal waves and river flows in the Yangtze Estuary, *Journal of Marine Systems*, 186, 17–28.